PNAS RESEARCH ARTICLE | MEDICAL SCIENCES

MDA-9/Syntenin in the tumor and microenvironment defines prostate cancer bone metastasis

Santanu Maji[a], Anjan K. Pradhan[a,b], Amit Kumar[a], Praveen Bhoopathi[a,b], Padmanabhan Mannangatti[a,b], Chunqing Guo[a,b,c], Jolene J. Windle[a,b,c], Mark A. Subler[a,b], Xiang-Yang Wang[a,b,c], Oliver J. Semmes[d], Julius O. Nyalwidhe[d], Nitai Mukhopadhyay[c,e], Asit Kr. Paul[c,f], Bryce Hatfield[g], Michael M. Levit[h], Esha Madan[b,c,i], Devanand Sarkar[a,b,c], Luni Emdad[a,b,c], David J. Cohen[h], Rajan Gogna[a,b,c], Webster K. Cavenee[j,1], Swadesh K. Das[a,b,c,1], and Paul B. Fisher[a,b,c,1]

Contributed by Webster K. Cavenee; received April 29, 2023; accepted September 25, 2023; reviewed by Kaustubh Datta, Martin G. Pomper, and Danyelle Townsend

Bone metastasis is a frequent and incurable consequence of advanced prostate cancer (PC). An interplay between disseminated tumor cells and heterogeneous bone resident cells in the metastatic niche initiates this process. *Melanoma differentiation associated gene-9* (*mda-9/Syntenin/syndecan binding protein*) is a prometastatic gene expressed in multiple organs, including bone marrow–derived mesenchymal stromal cells (BM-MSCs), under both physiological and pathological conditions. We demonstrate that PDGF-AA secreted by tumor cells induces CXCL5 expression in BM-MSCs by suppressing MDA-9-dependent YAP/MST signaling. CXCL5-derived tumor cell proliferation and immune suppression are consequences of the MDA-9/CXCL5 signaling axis, promoting PC disease progression. *mda-9* knockout tumor cells express less PDGF-AA and do not develop bone metastases. Our data document a previously undefined role of MDA-9/Syntenin in the tumor and microenvironment in regulating PC bone metastasis. This study provides a framework for translational strategies to ameliorate health complications and morbidity associated with advanced PC.

MDA-9/Syntenin | bone marrow–derived mesenchymal stromal cell | bone metastasis | PDGF-AA | CXCL5

In approximately 80% of prostate cancer (PC) patients, bone is the initial and primary metastatic site (1), affecting a patients' quality of life. Currently, advanced PC is incurable and results in significant disease morbidity and mortality (2). Bone metastasis involves dissemination of tumor cells toward bone, adherence to bone marrow cells, penetration/invasion into the bone marrow to the mineralized matrix, and growth of micrometastatic lesions (3). PC tumor cells deregulate the balance between bone formation (osteoblastic) and destruction (osteoclastic/osteolytic), resulting in weak (loss of mechanical strength) and fragile bones (4–8). Defining the molecular factors influencing this multistep process and the associated signaling pathways that are required for bone metastasis, but dispensable for normal bone physiology, could facilitate identification of potential "druggable" targets to effectively inhibit bone metastasis.

mda-9, also known as *Syntenin-1* (9) or *Syndecan Binding Protein* (referred to as *mda-9*), was initially cloned from terminally differentiating human melanoma cells (10, 11) and shown to positively regulate melanoma metastasis (12–15). A positive correlation was subsequently found between MDA-9 protein expression and cancer progression and poor prognosis in multiple cancer subtypes (reviewed in refs. 16 and 17), including PC (18, 19). Changes in signal transduction pathways are critical for the expression/secretion of metastasis-associated proteins that fuel the metastatic process. MDA-9 can also regulate metastasis in a tumor-cell independent (or extrinsic) manner (16). According to the human protein atlas (a Swedish-based program focused on mapping all the human proteins in cells, tissues, and organs; https://www.proteinatlas.org), this protein is widely expressed in all tissues and organs. To directly scrutinize the tumor cell-extrinsic role of MDA-9, we developed *mda-9/syntenin* global knockout animals (*mda-9*$^{-/-}$), which were viable, and analyzed the response to intravenously injected murine B16 melanoma cells (20). A lower incidence of lung metastasis in this animal model was observed, providing convincing support for our hypothesis that MDA-9 functions in both tumor cells and in the tumor microenvironment to promote the metastatic phenotype. This model is an excellent experimental tool for exploring the cell-intrinsic and cell-extrinsic roles of MDA-9 in multiple tumor types and has been used in our current study to dissect the critical steps in PC bone metastasis.

Cooperative interactions between tumor cells and bone resident cells are indispensable for progression of bone metastasis (21–23). Chemokines comprise a large and diverse group of small chemotactic proteins (8- to 11-KD), that together with their cognate

Significance

When prostate cancer (PC) advances, it predominantly metastasizes to bone where there are no effective therapies often culminating in patient death. PC progression is complex involving interactions between tumor cells and the microenvironment. Melanoma differentiation associated gene-9 (Syntenin-1. Syndecan Binding Protein) (MDA-9) is a unique prometastatic gene expressed in different organs, including bone marrow–derived mesenchymal stromal cells (BM-MSCs) under both physiological and pathological conditions. We document that MDA-9/CXCL5 signaling through PDGF-AA mediates PC proliferation and immune suppression, thereby facilitating bone metastasis. Our research extends the understanding of bone physiology as a consequence of metastasis and supports MDA-9 as a conceivable target for enhanced translational applications to ameliorate the health complications related with advanced PC.

Reviewers: K.D., University of Nebraska Medical Center; M.G.P., Johns Hopkins University; and D.T., Medical University of South Carolina.

The authors declare no competing interest.

[1]To whom correspondence may be addressed. Email: wcavenee@health.ucsd.edu, swadesh.das@vcuhealth.org, or paul.fisher@vcuhealth.org.

This article contains supporting information online at https://www.pnas.org/lookup/suppl/doi:10.1073/pnas.2307094120/-/DCSupplemental.

Published November 3, 2023.

receptors, play key roles in adherence of tumor cells to endothelium, extravasation from blood vessels, metastatic colonization, angiogenesis, and proliferation of numerous tumor types (24). Chemokines produced by tumors, such as CCL2, CCL3, IL-8/CXCL8, and CXCL12, are involved in regulating tumor growth and bone remodeling (25). However, bone marrow–produced cytokines, like mesenchymal stem cell–derived CCL5, also promote tumor cell metastasis (26). CXCL12, which is a homeostatic chemokine secreted by stromal cells in the bone marrow, is elevated in metastatic tissues of PC (27). CXCL5 is a member of the angiogenic CXC chemokine family and overexpression of CXCL5 occurs in several human tumors such as head and neck squamous cell carcinoma, gastric, pancreatic, colorectal, and prostate and lung cancer, as well as in lung tissue of patients with pulmonary fibrosis (28). High CXCL5 expression is associated with prostate tumor progression and inflammatory infiltration (29). Exogenous administration of CXCL5 stimulates highly aggressive PC cells to invade through a synthetic basement membrane in vitro (30). Macrophage-driven efferocytosis of PC apoptotic cells induces the expression of CXCL5 by activating Stat3 and NF-κB (p65) signaling (29). High levels of CXCL5 are found in the serum of advanced-stage cancer patients and correlate with vascularity of tumors and immunomodulation (31–33). In this study, we tested the hypothesis that expression of *mda-9/syntenin* in noncancerous cells, such as bone marrow–derived mesenchymal stromal cells (BM-MSCs), facilitates metastatic progression by up-regulating CXCL5 expression in the local tumor environment, thereby fostering tumor cell homing and expansion, and modulating bone homeostasis.

Results

Physiological Expression of *mda-9* Regulates Bone Metastasis Progression. A variant of murine RM1-*Luc* (stably expressing *Luciferase*) PC cells (34), RM1-BM-*Luc*, with an enhanced propensity to form bone metastases was developed. In vivo, this cell line forms osteolytic tumors with osteoblastic changes (35). Intracardiac injection of RM1-BM-*luc* cells in wild-type (WT, *mda-9*$^{+/+}$) and KO (*mda-9*$^{-/-}$) mice (20) (lack of *mda-9/syntenin* expression in all organs including the bone niche) caused bone metastases in approximately 70% of WT mice (5 out of 7), whereas no bone metastases developed in *mda-9*$^{-/-}$ mice (0 out of 7) (Fig. 1*A*). These data support a putative role of *mda-9/syntenin* when expressed in the microenvironment (bone niche) in controlling bone metastasis. μCT quantification of femurs revealed decreased cortical bone volume and trabecular bone thickness, and an increase in trabecular number in tumor-bearing WT compared to naïve controls and *mda-9*$^{-/-}$ mice (*SI Appendix*, Fig. S1*A*). To determine the effect of MDA-9/Syntenin expression on multiorgan metastasis, a different cohort (n = 5) of animals were killed after 15 d and examined for the presence of metastases in multiple tissues. The lack of *mda-9/syntenin* expression also reduced global metastatic events, documented by both BLI (Fig. 1*B*) and microscopically (Fig. 1*C*), in the lungs, brain and liver, and this lower incidence of metastasis correlated with enhanced animal survival (Fig. 1*D*). Autologous transfer of wild-type bone marrow reversed resistance to bone metastasis development in *mda-9*$^{-/-}$animals (Fig. 1*E*). Two out of three recipient *mda-9*$^{-/-}$ mice developed bone metastasis, vs. no bone metastasis in *mda-9*$^{-/-}$ mice receiving sham transfusion

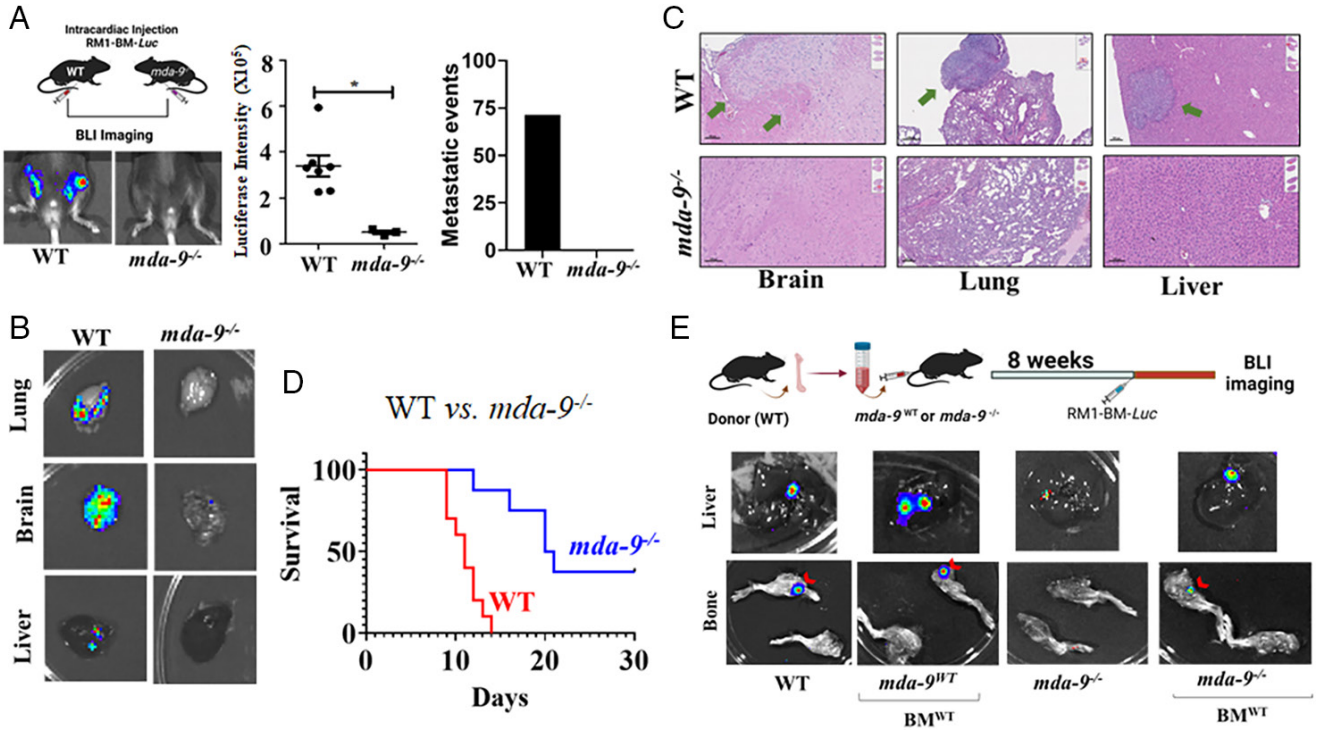

Fig. 1. Global *mda-9/syntenin* knockout (*mda-9*$^{-/-}$) animals are innately resistant to bone metastasis. (*A*) A total of 3 × 10^4 RM1-BM-*Luc* cells were injected by the intracardiac route (I.C.) into wild-type C57BL/6 (WT) and *mda-9*$^{-/-}$ mice. BLI imaging was performed at day 14 to monitor bone metastasis. Representative BLI images from each experimental group are presented. Luciferase intensity was calculated using built-in Living Image Software v.2.50, and the average value for each group is graphically presented. Region of interest (ROI) was calculated and graphed based on imaging (*Middle*). Metastatic events in femurs were identified based on BLI imaging at a single time point, and percentage (n = 7) effects are presented (*Left*). (*B* and *C*) Representative ex vivo BLI photomicrographs and corresponding H/E stained sections of different organs from RM1-BM1-*Luc* implanted (I.C.) WT and *mda-9*$^{-/-}$ animals. In *C*, the tumor is indicated by an arrow. (*D*) Kaplan–Meier curve showing overall survival of tumor-bearing animals from different genetic backgrounds. *$P < 0.05$. (*E*) Schematic diagram for the bone marrow transfusion protocol is described in the upper panel. Briefly, whole bone marrow cells were obtained from WT mice (BM^{WT}) and injected into age-matched prior irradiated (at 10 Gy) WT and *mda-9*$^{-/-}$ mice. The "Sham Transfusion" group received bone marrow culture media only. After 8 wk, all mice were challenged with RM1-BM-*Luc* (I.C.). Representative ex vivo image (liver and bone) for each experimental group is presented in the lower panel. *Statistically significant ($P < 0.05$).

(0 out of 5). These data suggest enhanced remodeling of bone in WT mice following exposure to PC cells. It was necessary to euthanize WT and KO recipient mice that received autologous WT bone marrow earlier than controls (sham controls) or KO animals without transfusion due to multiorgan metastases, including lung, brain, and liver (*SI Appendix*, Fig. S2).

A surgical bone implantation approach (described in *Materials and Methods*) was used to examine the impact of RM1-BM-*Luc* tumor growth and to study the tumor-bone interface in *mda-9*$^{-/-}$ animals (36). The absence of *mda-9/syntenin* profoundly affected tumor growth (Fig. 2*A*). Cortical thinning was observed in both WT and *mda-9*$^{-/-}$ femurs, as well as trabecular resorption compared to contralateral control legs that did not receive RM1-BM-*Luc* cells (Fig. 2*B*). Moreover, tumor growth in WT mouse femurs resulted in pathologic fractures in 3/6 animals, while no fractures were observed in *mda-9/syntenin* knockout mice (Fig. 2*C*), suggesting that MDA-9/Syntenin enhances the rate and amount of osteolysis. Failure of tumor growth was further confirmed by lack of KI-67 (proliferation marker) positivity in tumors in the *mda-9*$^{-/-}$ bone niche compared to WT animals. (Fig. 2*D*). In support of the in vivo findings, the proliferation of RM1-BM-*Luc* cells was reduced when cocultured with bone marrow (BM) from *mda-9*$^{-/-}$ mice as compared with WT bone marrow cells (Fig. 2*E*). Collectively, our observations support the hypothesis that the lack of *mda-9/syntenin* in the host bone microenvironment has a protective effect following exposure to PC cells.

CXCL5 Expression Is Linked with PC Disease Status. Serum samples from animals injected with PC tumor cells (WT and *mda-9*$^{-/-}$) were screened using a protein-based chemokine array (Fig. 3*A* and *SI Appendix*, Fig. S3*A* and Table S1). CXCL5 was the most robustly down-regulated chemokine in *mda-9*$^{-/-}$ animals. Validation of array data was obtained using serum from animals with and without tumors. Tumor implantation increased CXCL5 serum levels (as compared to basal levels) specifically in WT animals. Serum from *mda-9*$^{-/-}$ animals did not contain increased CXCL5, suggesting an innate impairment of CXCL5 expression in response to PC tumor cells in *mda-9*$^{-/-}$ mice (Fig. 3*B*). Since a robust downregulation of this protein is observed in *mda-9*$^{-/-}$ animals after implanting PC tumor cells, we postulate that the differential expression of CXCL5 is directed by MDA-9 expression. We cocultured freshly isolated BM obtained from either WT or *mda-9*$^{-/-}$ animals with RM1-BM-*Luc* cells (Fig. 3*C*) and two additional murine PC lines that promote bone metastases, TRAMP-C2- (37) and B6CaP- (38) derived conditioned media (*SI Appendix*, Fig. S3*B*). A >twofold enhanced expression of CXCL5 mRNA was observed within 12 h. in WT but not in *mda-9*$^{-/-}$ BM, firmly establishing CXCL5 regulation by an *mda-9*-dependent pathway. In addition, CXCL5 expression was restored in response to tumor cells in *mda-9*$^{-/-}$ mice receiving autologously transferred BM-MSCs from WT mice (Fig. 3*D*), and this restoration correlated with PC progression and development of bone metastasis (Fig. 1*E*). Multicolor FACS analyses indicated that bone marrow–derived mesenchymal stromal cells (BM-MSCs, characterized with CD45^{-}CD90^{+}) (Fig. 3*E*), but not macrophages, dendritic or natural killer cells (*SI Appendix*, Fig. S3*C*), from WT mice differentially express CXCL5 in response to tumor cells. All of these cell types from *mda-9*$^{-/-}$ mice do not respond to tumor cells in terms of CXCL5 expression, further confirming dependence of *mda-9/syntenin* in this pathway. It is worth noting that neither WT (*mda-9*$^{+/+}$) nor *mda-9*$^{-/-}$ BM-MSCs responded to other chemokines such as CXCL10 or CCL-11 (two other down-regulated chemokines) (*SI Appendix*, Fig. S3*D*). Immunofluorescence staining confirmed strong coexpression of CD90 and CXCL5 (Fig. 3*F*, merge panel) providing additional support for BM-MSCs as a source

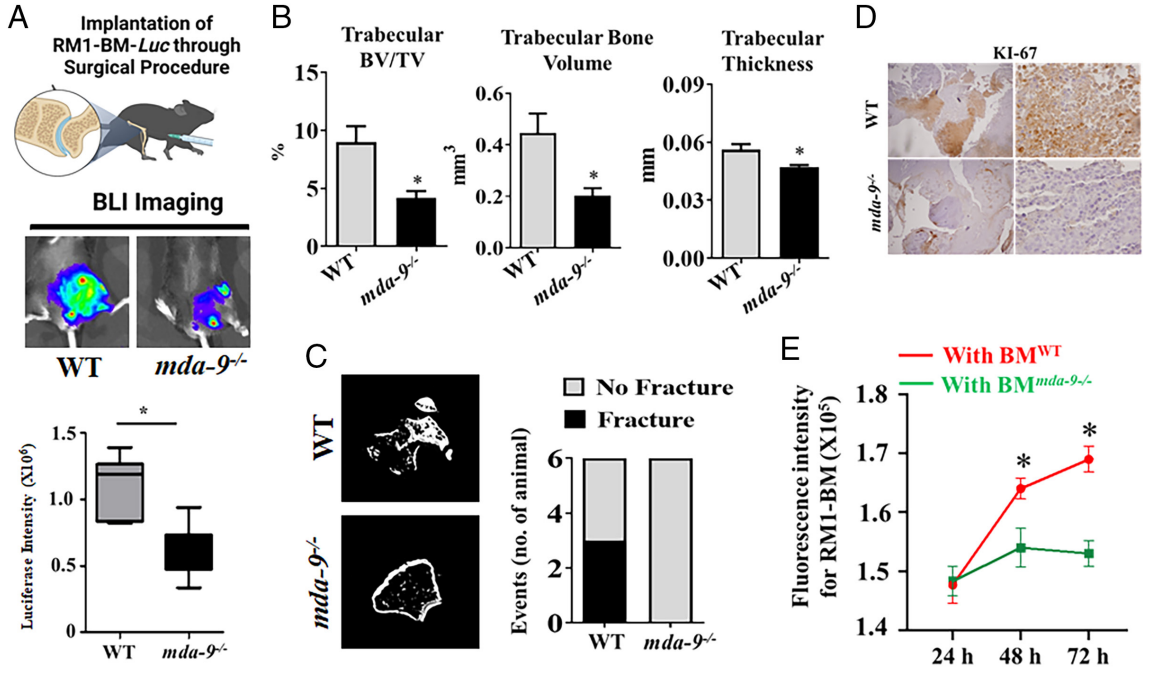

Fig. 2. Lack of MDA-9/Syntenin expression inhibits tumor outgrowth in the bone niche. (*A*) RM1-BM-*Luc* cells were directly implanted (into the femur) in 2-mo-old WT and *mda-9*$^{-/-}$mice (*Top* panel: schematic presentation). Representative images at day 14 are presented (*Middle*). Luciferase intensity was calculated using built-in Living Image Software v.2.50, and the average value for each group at day 14 is graphically presented (*Bottom*). Error bars ± SD. (*B*) Quantification of mineralized tissue by μCT in the distal femur. Femurs were assessed for amount of trabecular bone volume over total volume, bone volume alone, and thickness of the trabeculae in the distal femur. (*C*) Prevalence of pathologic fracture as observed by μCT. (*D*) Tumor-implanted bones (from animals studied in panel *A*) were immunostained for KI-67 expression, and the representative photographs at lower (*Left*) and higher magnifications (*Right*) are presented. (*E*) Bone marrow cells from WT (BM^{WT}) and *mda-9*$^{-/-}$ (BM$^{mda\text{-}9^{-/-}}$) mice were isolated and cocultured with fluorescently labeled tumor cells (RM1-BM-*Luc*) and incubated for different time periods. FACS analyses were performed to detect tumor cells at different time points. *Statistically significant ($P < 0.05$).

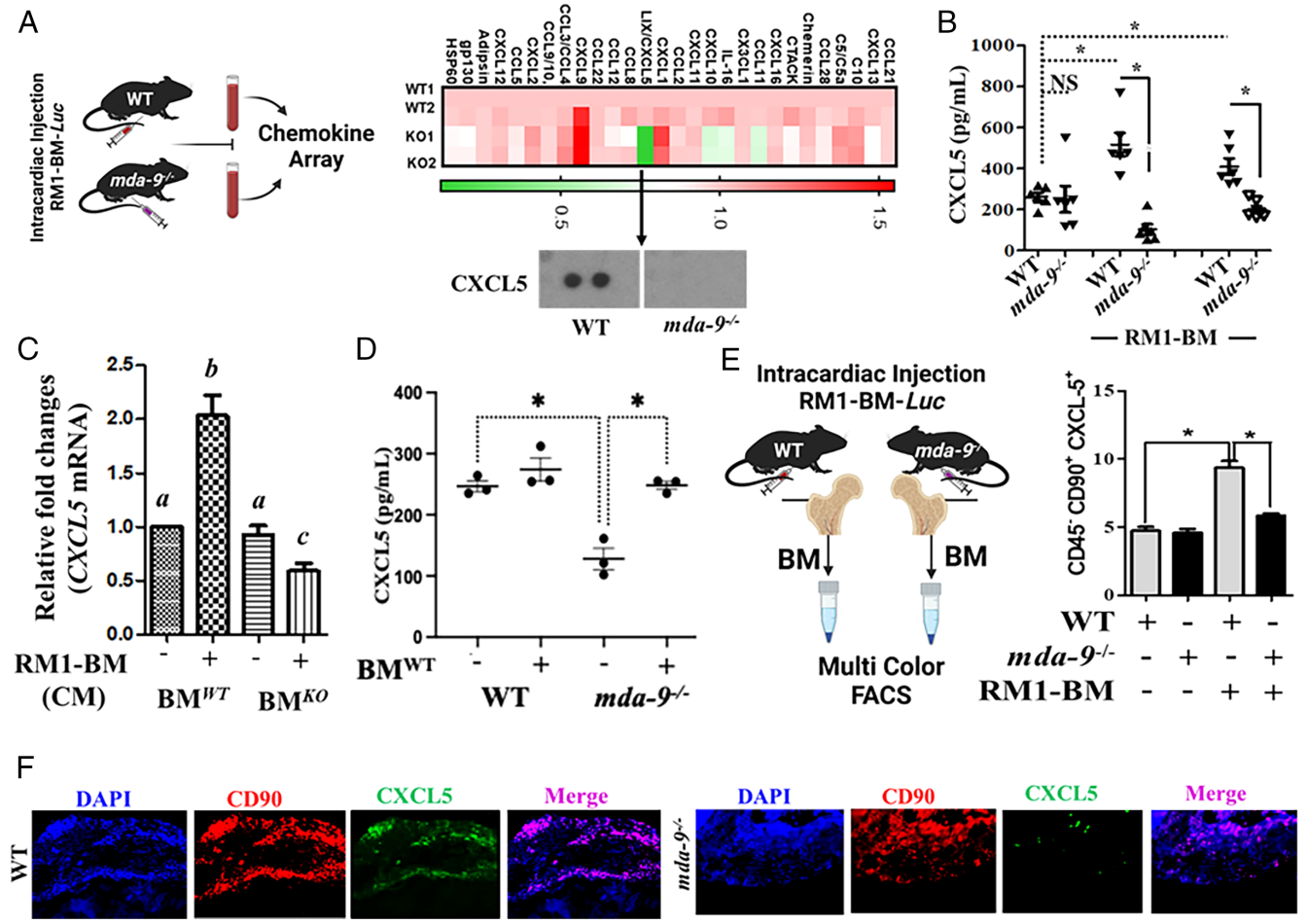

Fig. 3. CXCL5 expression correlates positively with bone metastasis progression. (*A*) Serum samples were isolated from tumor-bearing mice [14 d after intracardiac (I.C.) injection, 3×10^4 cells/mouse], and protein-based arrays were analyzed as described by R&D Biosystems. Heatmap is presented. Cropped blot for CXCL5 is presented in the bottom panel. (*B*) CXCL5 level in serum from mice under different experimental conditions (sham/basal level vs. 14-d post-I.C. or postorthotopic implantation (1×10^4 cells/mouse). A mouse-specific CXCL5 enzyme-linked immunosorbent assay (ELISA) kit (R&D Biosystems) was used for determining CXCL5 levels. (*C*) Bone marrow (BM) cells were isolated from WT (BM^{WT}) and *mda-9*$^{-/-}$ (BM^{KO}) mice and stimulated with tumor cell–derived conditioned media for 12 h. Total cellular RNA was extracted, and qPCR was performed to detect mouse *CXCL5* mRNA. Data are presented as fold-change relative to the unstimulated wild-type (BM^{WT}) group. Different letters in two variables are statistically significant ($P < 0.05$). (*D*) CXCL5 levels in serum from tumor-bearing mice receiving "sham" (represented as "–") or "WT" (represented as "+") bone marrow (experiments described in Fig. 1*E*). *$P < 0.01$. (*E*) A total of 3×10^4 RM1-BM-*Luc* cells were injected by the intracardiac (I.C.) route into WT and *mda-9*$^{-/-}$ mice (schematically presented in the left panel). Fourteen days postinjection, total BM cells were isolated and stained for lineage-specific cell surface markers and intracellular CXCL5 expression to identify the specific cell population(s) that differentially respond to tumor cells. Percentages of CXCL5 expression in bone marrow–derived mesenchymal stromal cells: ($CD45^-CD90^+$) are presented. *$P < 0.05$. (*F*) Tumor-implanted bones (from animals in Fig. 2*A*) were immunostained with different antibodies as indicated, and representative photographs are presented.

of CXCL5. A putative role of CXCL5 in metastasis is predicted based on prior research (29, 30). Initial experiments were designed to confirm a role for CXCL5 in tumor growth in the bone niche using an interfemoral experimental model and to determine whether CXCL5 expression could directly affect tumor growth and elicit therapeutic responses. CXCL5 was neutralized with anti-CXCL5 (30 min) after PC tumor cell implantation and animals received two additional doses on the subsequent second and third day. Tumor growth was significantly inhibited following CXCL5 neutralization (*SI Appendix*, Fig. S4) supporting a role of CXCL5 in tumor growth.

Defining a Regulatory Role of Mda-9/Syntenin in CXCL5 Expression in Human PC. A subline of PC-3 cells that preferentially metastasizes to bone following intracardiac injection, PC-3ML, provides an additional model to study PC bone metastasis (39, 40). Using the CRISPR approach to knockout *mda-9* in PC-3ML cells (lack of MDA-9 expression was confirmed, *SI Appendix*, Fig. S5*A*), in vivo PC bone metastasis was significantly inhibited (Fig. 4*A*). Eighty percent of WT animals (8/10) developed bone metastases within 36 d following intracardiac injection of parental PC-3ML cells. At this time point, significantly fewer $PC\text{-}3ML^{mda\text{-}9\ KO}$ injected animals (2/10) had metastatic lesions in bone (Fig. 4*A*). These data strongly support a tumor autonomous/nonautonomous role of MDA-9/Syntenin in defining metastatic competence. Interestingly, conditioned media (CM) from PC-3ML but not $PC\text{-}3ML^{mda\text{-}9\ KO}$ cells induced CXCL5 expression in HS5 cells (Fig. 4*B*). Since the changes occurred at the transcriptional level (*SI Appendix*, Fig. S5*B*), shown using an ~1.5-kb *CXCL5* Promoter reporter construct (*CXCL5*-Prom), we confirmed that tumor cell–derived CM mediated CXCL5 regulation at the gene promoter level (Fig. 4*C*).

Macrophage-driven efferocytosis of PC apoptotic cells induces expression of CXCL5 by activating STAT3 and NF-κB (p65) signaling (29). Hyperactivated Hippo-YAP, signaling through CXCL5 in PC tumors, results from the YAP-TEAD complex promoting myeloid-derived suppressor cell (MDSC) recruitment (41). Considering the pivotal role of the Hippo pathway (shown schematically in *SI Appendix*, Fig. S5*C*) in CXCL5 regulation, (41) HS5 cells [human bone marrow–derived mesenchymal

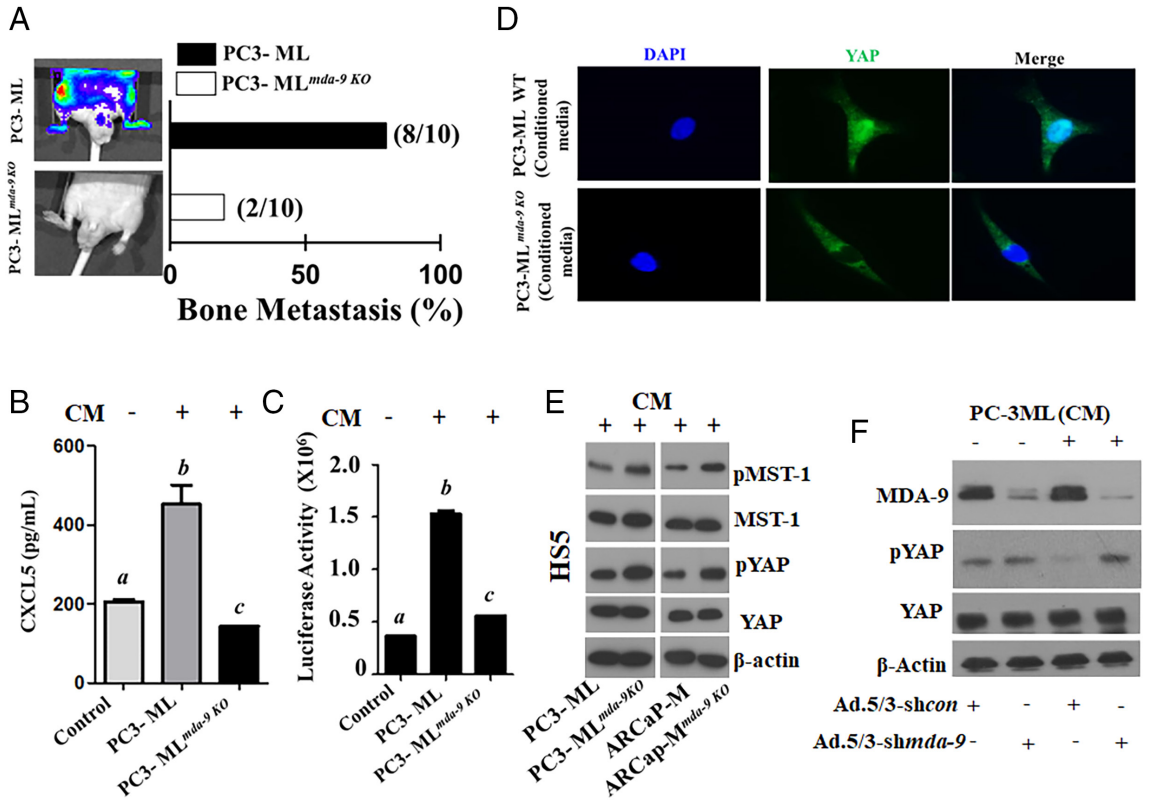

Fig. 4. MDA-9 expression in tumor cells nonautonomously activates the Hippo pathway and induces CXCL5 in HS5 cells. (*A*) Bone metastasis development in athymic nude mice following intracardiac injection of PC-3ML control and *mda-9* KO (PC-3ML$^{mda\text{-}9\ KO}$) clone (1 × 10^5 cells/mouse). Representative images 36 d after tumor cell implantation (*Left*). Bone metastases detected by BLI imaging. The percentage of mice with BLI-positive lesions is shown (*Right*). (*B*) HS5 cells were incubated with normalized (equal amount of total protein) tumor cell–derived condition media for 12 h. HS5-derived conditioned media were analyzed for CXCL5 levels using ELISA. (*C*) HS5 cells were transfected with a 1.5-kb CXCL5-*Prom* using a standard transfection protocol. Twelve hours posttransfection, cells were stimulated with conditioned media for an additional 12 h. Luciferase activity was measured and presented after normalizing with *Renilla luciferase*. (*D*) HS5 cells were incubated with tumor cell–derived conditioned media for 12 h and stained with fluorescently labeled anti-YAP. DAPI was used for nuclear staining. Translocation of YAP into the nucleus was monitored under a fluorescence microscope. (*E*) HS5 cells were incubated with tumor cell– (parental and its *mda-9* knockout variant) derived conditioned media for 12 h, and cell lysates were analyzed for different proteins, as indicated. (*F*) MDA-9/Syntenin expression was knocked down in HS5 cells using an Adenovirus expressing sh*mda-9*. Twenty-four hours postinfection, culture media were replaced with fresh media containing PC-3ML CM for an additional 12 h. Cell lysates were analyzed for the indicated proteins. Different letters in two variables are statistically significant ($P < 0.05$).

stromal cells (MSCs); emulating the effect of MSCs on regulating tumor progression (42)] were incubated with either CM from parental or *mda-9/syntenin* KO PC3-ML cells. Failure of YAP translocation into the nucleus in HS5 cells after treatment with *mda-9/syntenin* KO CM suggests "Hippo On" (Fig. 4*D*), which was confirmed by upregulation of phosphorylation of both MST and YAP in cell lysates. Phosphorylation promotes cytoplasmic localization and inhibits nuclear translocation (41). CM from the *mda-9* KO line significantly up-regulated phosphorylation of MST and YAP, which are important inhibitors of translocation (Fig. 4*E*). To understand the dependency of MDA-9/ expression on Hippo signaling (YAP phosphorylation), we down-regulated MDA-9 expression [using a chimeric adenovirus 5/3 expressing sh*mda-9;* Ad.5/3-sh*mda-9* (13)] in HS5 cells and then stimulated with PC3-ML CM. PC-3ML-derived CM inhibited phosphorylation of YAP only when MDA-9 was expressed in stromal cells (Fig. 4*F*).

Further confirmation that tumor cell–derived CM induces CXCL5 through the Hippo pathway was obtained by treating HS5 cells with CM after modulating different components of the Hippo pathway, e.g., MST1 and YAP (Fig. 5 *A, i–v*). PC3-ML CM induced CXCL5 secretion from HS5 cells, but overexpression of MST1 significantly attenuated PC3-ML CM induced CXCL5 secretion (Fig. 5 *A, ii*). Overexpression of a catalytically inactive MST1 K59R (MST1-Ki) (43) reversed inhibition of CXCL5 secretion in HS5 cells (Fig. 5 *A, iii*). Similarly, genetic inhibition of YAP reversed PC3-ML CM induced CXCL5 secretion in HS5 (Fig. 5 *A, iv*). Additionally, overexpression of YAP in HS5 cells induced CXCL5 promoter activity (Fig. 5 *A, v*). Substantial nuclear localization of YAP was evident in RM1-BM tumor-bearing bone sections (Fig. 5*B*) from WT but not KO animals. To identify the CXCL5 promoting factor(s), we fractionated PC-3ML CM and determined the activity of the *CXCL5*-Prom when transfected into HS5 cells. This study suggested putative factor(s) between 10 and 30 kDa could regulate CXCL5 expression (Fig. 5*C*).

Conditioned media derived from *mda-9*$^{-/-}$ PC3-ML cells (PC3-ML$^{mda\text{-}9\ KO}$) fail to activate the CXCL5 promoter (Fig. 4*B*), which correlates with bone metastasis development in nude mice (Fig. 4*A*). For further analysis, we compared growth factor arrays using parental (PC3-ML) vs. *mda-9* KO PC3-ML cell-CM. This experiment documented differential expression of PDGF-AA, GM-CSF, and IGFBP-4 (Fig. 6*A* and *SI Appendix*, Fig. S6*A* and Table S2). We tested these three growth factors for their ability to stimulate CXCL5 in HS5 cells. PDGF-AA significantly induced CXCL5 (Fig. 6*B*) through promoter activation (Fig. 6*C*), while GM-CSF and IGFBP4 demonstrated a minimal effect (*SI Appendix*, Figs. S6*B* and S7*A*). CM and its active fraction from PC-3ML cells stimulated CXCL5 expression, which was blocked by neutralizing PDGF-AA (Fig. 6*D* and *SI Appendix*, Fig. S7*B*). This is a demonstration of a role of MDA-9 in promoting PDGF-AA expression. We confirmed PDGF-AA regulation by MDA-9 in PC3-ML and two additional human PC lines, PC-3 and ARCaP-M

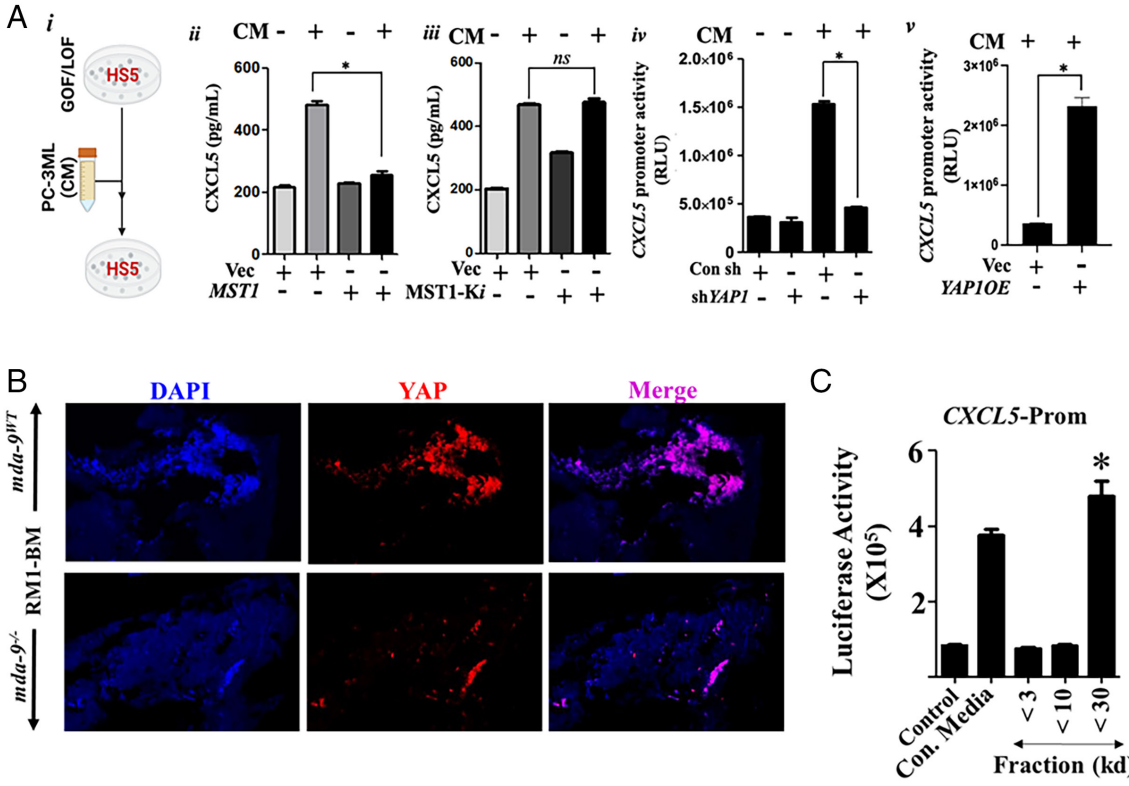

Fig. 5. Hippo pathway activates CXCL5 in HS5 cells. (*A*) Panel *i* Schematic representation of the experimental protocol used in panels *ii–iv*. Different overexpression/siRNAs (GOF/LOF) constructs were transfected into the indicated cells, and after 24 h, tumor-derived condition medium was used to stimulate HS5 cells for an additional 12 h. Panels *ii* and *iii* represent CXCL5 expression in HS5-derived conditioned media, determined by ELISA. Panels *iv and v* show CXCL5 promoter activity. In this experiment, HS5 cells were cotransfected with both CXCL5-*Prom* and either shYAP1 or YAP1 OE vectors before treating with conditioned media. *=*P* <0.05. (*B*) YAP expression was analyzed in paraffin sections (tumor-bearing bones from the experiment performed in Fig. 2*A*). (*C*) HS5 cells were incubated with different fractions of PC-3ML-derived conditioned media for 24 h after initial transfection with a *CXCL5*-Prom. Luciferase activity was measured and presented after normalizing with *Renilla luciferase*. **P* <0.05.

(18) using multiple knockout clones (Fig. 6*E*) with MDA-9 down-regulation and restoring *mda-9* in KO clones using Ad.5/3-*mda-9* to restore PDGF-AA expression (Fig. 6*F*). Our in vitro studies indicate that PDGF-AA down-regulates phosphorylation of MST1 and YAP, two essential proteins involved in Hippo signaling in HS5 cells (Fig. 6*G*). Additionally, PDGF-AA induced CXCL5

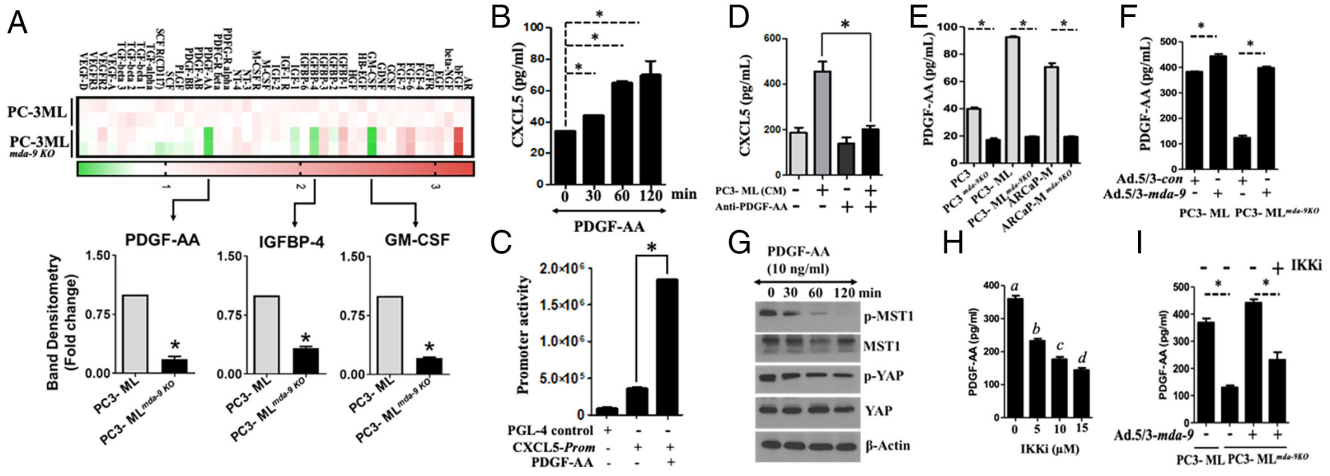

Fig. 6. Tumor cell–derived PDGF-AA induces CXCL5 expression in HS5 cells. (*A*) Normalized (based on equal amounts of total protein) conditioned media, isolated from parental and knockout variants, were subjected to protein-based growth factor arrays as described by Ray Biotech. Heatmap is presented. Densitometry analyses (n = 2, for corresponding proteins) were performed for each growth factor, and the data are presented only for three. (*B*) HS5 cells were treated for the indicated times with PDGF-AA, and CXCL5 protein expression was determined. (*C*) HS5 cells were transfected with a 1.5-kb CXCL5-*Prom* using a standard transfection protocol. Twelve hours posttransfection, cells were treated with PDGF-AA for an additional 12 h. Luciferase activity was measured and presented after normalizing with *Renilla luciferase*. (*D*) PC-3ML-derived conditioned media were incubated with control IgG or anti-PDGF-AA before treatment of HS5 cells for 12 h, and CXCL5 levels were measured in media. (*E*) Expression of PDGF-AA was determined in the indicated tumor cells and corresponding *mda-9* knockout clones. (*F*) Cells were infected with an Adenovirus expressing control or *mda-9* overexpressing construct for 24 h, and PDGF-AA expression in media was determined using ELISA. (*G*) HS5 cells were treated with PDGF-AA and analyzed for expression of the indicated proteins. (*H*) Tumor cells were cultured in the presence or absence of IKK2i for 12 h and analyzed for expression of the indicated proteins. Different letters in two variables are statistically significant ($P < 0.05$). (*I*) MDA-9 was knocked-into PC-3ML$^{mda\text{-}9\ KO}$ cells and cultured for an additional 12 h in the presence or absence of IKK2i. PDGF-AA was determined using ELISA. *=$P < 0.05$.

promoter activity in an NF-κB-dependent pathway (Fig. 6*H*), and the activation was partially regulated by MDA-9 (Fig. 6*I*). It is worth noting that PDGF-AA expression is complex and can be regulated by multiple pathways (*SI Appendix*, Fig. S7*C*) including the Akti-1/2 or PI3K pathway.

PDGF-AA-mediated upregulation of CXCL5 was not apparent in HS5 cells when *mda-9* expression was blunted using sh*mda-9* (Fig. 7*A*). As predicted, *mda-9* manipulated HS5 cells were less responsive to PDGF-AA-mediated signaling, as confirmed by reduced phosphorylation of PDGFR-α (Fig. 7*B*). Addition of recombinant PDGF-AA to PC-3ML$^{mda\text{-}9KO}$ CM restored the suppressive effect of PDGFR and its downstream Hippo pathway. (Fig. 7*C*). Similar to the human cell–derived data, mouse PDGF-AA induced CXCL5 expression in wild-type, but not in *mda-9*$^{-/-}$ BM-MSCs (Fig. 7*D*). Similar to the human cell–derived data, mouse PDGF-AA induced CXCL5 (and minimally *CXCL10* and *CXCL11*) expression in wild-type, but not in *mda-9*$^{-/-}$ BM-MSCs (Fig. 7*D* and *SI Appendix*, Fig. S8). Further support for MDA-9-mediated PDGF/PDGFR signaling comes from examining tumor-bearing bone sections where phosphorylation of PDGFR was significantly reduced in *mda-9* KO animals (Fig. 7*E*). Collectively, these data reveal a function of MDA-9 in BM-MSCs that regulates PDGF signaling.

We next examined the expression of CXCL5 in tumor from patients with bone metastases using human-specific antibody (Fig. 8*A*). The H score for tumor and stroma (Fig. 8*B*) was calculated and supports CXCL5 expression in both compartments, i.e., tumor and stroma (Fig. 8*C*). Coculturing PC3-ML (at different ratios) with HS5 cells confirm an enrichment of CXCL5 expressing cells (Fig. 8 *C*, *Left* and *Right* panel for tumor and stromal cells, respectively) and secretion (in cocultured conditioned media, Fig. 8 *C*, *Right* panel) further validating our observations in clinical samples, i.e., both compartments are expressing CXCL5. Clinically, both PDGF-AA and CXCL5 proteins are significantly up-regulated in patients with advanced-stage PC (PathStage T3b or T3c, Gleason Score >7) and PC patients with reported bone metastases in comparison to nontumor populations (with benign/ atrophy, clinical stage T0) (Fig. 8*D*). Using a linear regression analysis, PDGF-AA is a statistically significant predictor of CXCL5, at a 5% level of significance (F test *P* value < 0.001). These results provide support for our hypothesis that MDA-9 is obligatory for CXCL5 expression in response to tumor-derived growth factor(s) (e.g., PDGF-AA) (Fig. 8*D*). All clinical information (both paraffin-embedded sections and serum are provided in *SI Appendix*, Tables S3 and S4).

Discussion

Paracrine loops between bone matrix–derived growth factors are pivotal for PC bone colonization and remodeling during PC metastasis (44, 45). A complex interplay exists between tumor cells that express receptors that favor chemotaxis and the host environment where proper cell–cell engagement is obligatory for the release of cytokines and growth factors (25). Current studies delineate MDA-9's contributions to the cooperative interactions

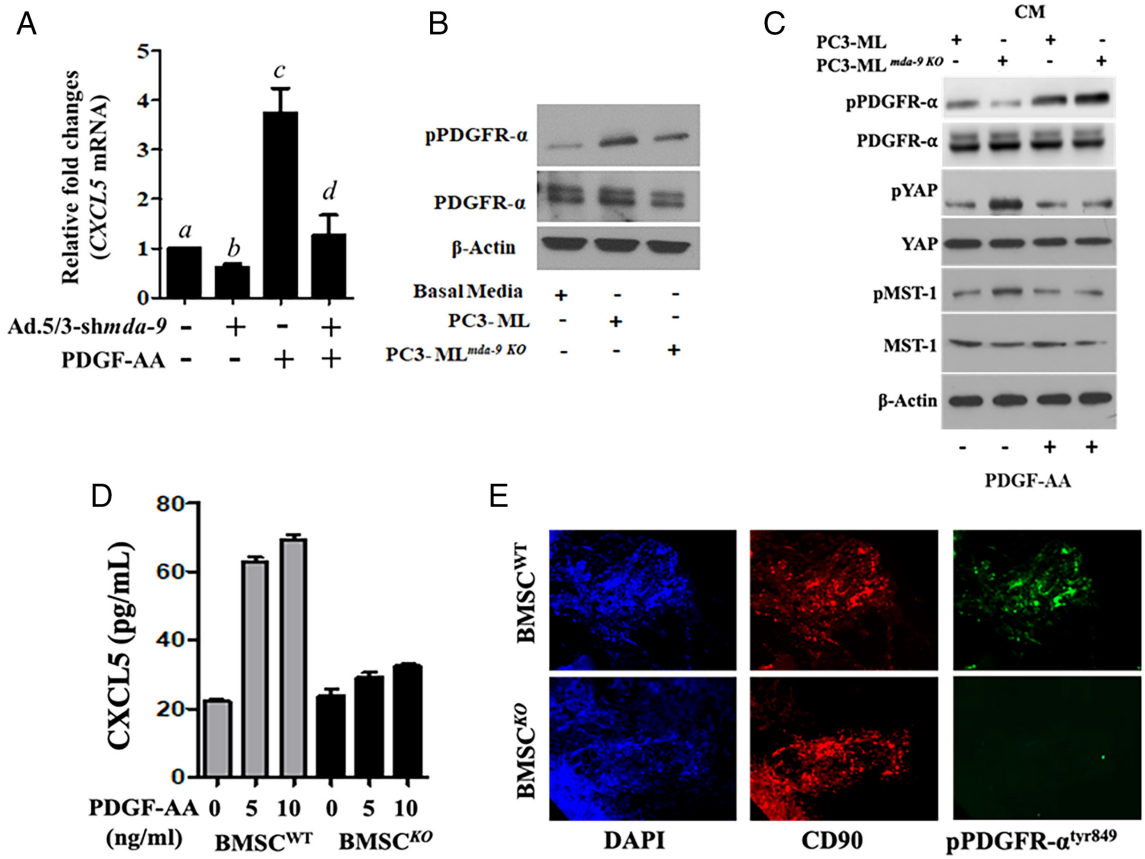

Fig. 7. MDA-9 expression in HS5 regulates PDGF/PDGFRα signaling. (*A*) *mda-9* expression was blunted, and 24 h postinfection, HS5 cells were stimulated with PDGF-AA for an additional 12 h. mRNA for CXCL5 expression was analyzed using qPCR. Different letters in two variables are statistically significant ($P < 0.05$). (*B*) HS5 cells were incubated with media supplemented with the indicated tumor cell–derived conditioned media for 12 h, and western blotting was done for phosho-PDGFRα and total PDGFR. (*C*) HS5 cells were incubated with media supplemented with the indicated tumor cell–derived conditioned media and PDGF-AA for 12 h, and western blotting was done for the indicated proteins. (*D*) BM-MSCs from WT and *mda-9*$^{-/-}$ mice were stimulated with mouse PDGF-AA, and CXCL5 expression was determined in the culture media. (*E*) phospho-PDGFR expression was analyzed in paraffin sections (tumor-bearing bone from the animal experiment, described in Fig. 2*A*). Different letters in two variables are statistically significant ($P < 0.05$).

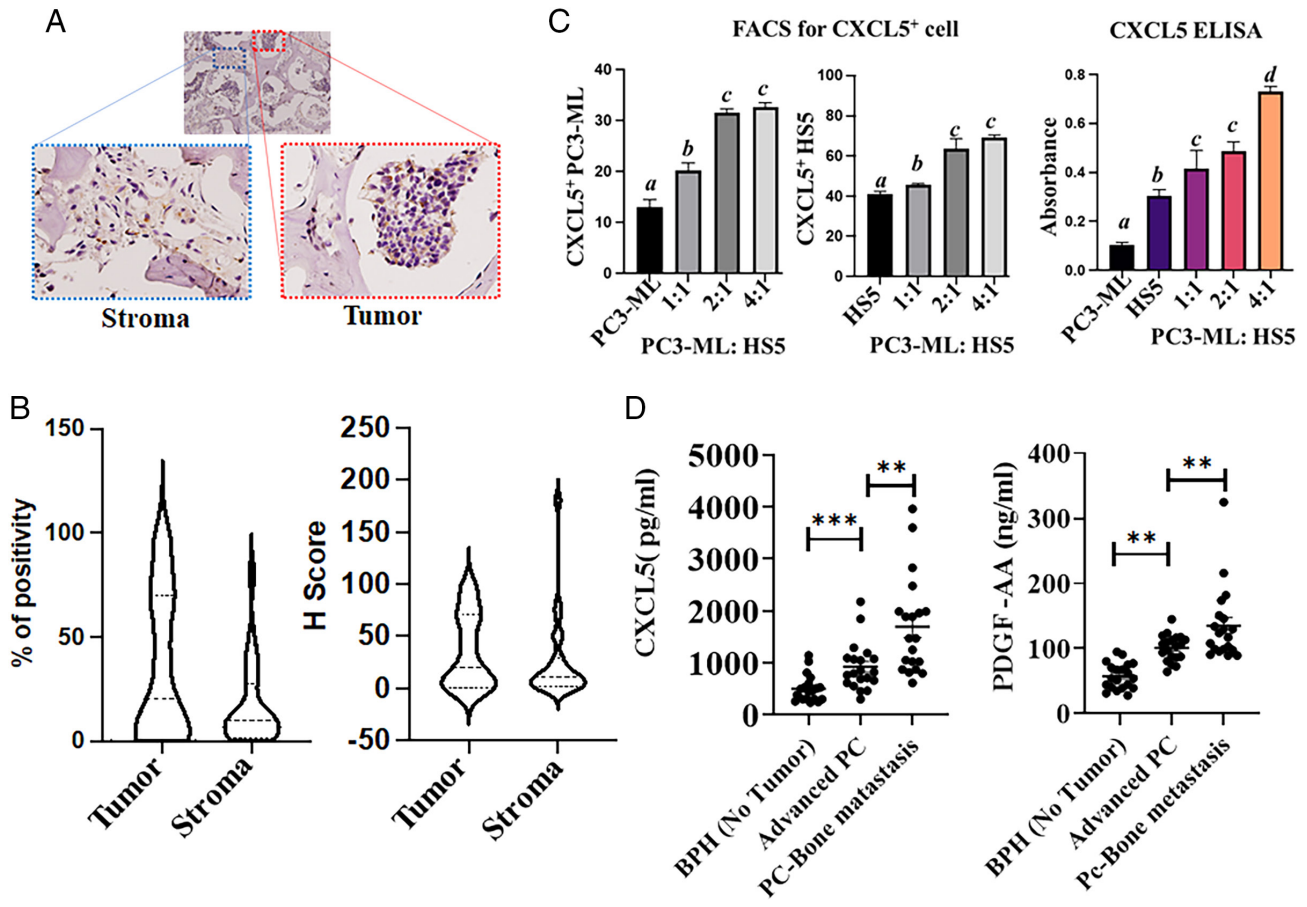

Fig. 8. CXCL5 is expressed in both stroma and tumor cells. (*A*) Paraffin-embedded section from a patient with metastatic PC bone metastasis was immunostained with anti-CXCL5, and the expression in the stroma and tumor compartment is presented in the *Inset*. (*B*) H-Score was determined by an anatomic pathologist based on staining intensity, and values are presented. (*C*) PC3-ML cells were stained with CytoTrack™ Red and cocultured with of HS5 cells. After 24 h, cells were stained with CXCL5-FITC and analyzed by FACS [the left panel represents double staining (tumor cell-Red and CXCL5-FITC)]; the middle panel is for only CXCL5-FITC (only HS5). The right panel represents conditioned media that were collected from the above indicated PC3-ML and HS5 cocultured cells, and secretion of CXCL5 was measured by ELISA. (*D*) Human serum samples from the indicated patient groups were analyzed for PDGF-AA and CXCL5 (n = 20). Different letters in two variables are statistically significant ($P < 0.05$). *Statistically significant. **$P < 0.001$.

between disseminated tumor cells and BM-MSCs, establishing MDA-9/PDGF-AA/CXCL5 as a key signaling pathway regulating PC bone metastasis (Summarized in Fig. 9).

Successful metastatic colonization requires complex collaborations between the tumor and local environment (3, 46). Using murine and human immortalized BM-MSCs, we demonstrate that MDA-9/Syntenin expression is pivotal to CXCL5 production in response to tumor cell–derived growth factors. CXCL5 induction is critical not only for tumor cell chemotaxis (29) but also contributes to the structure of the microenvironment that facilitates lesion outgrowth (29, 30). Support for this supposition is provided using neutralizing antibody (*SI Appendix*, Fig. S4). In advanced PC, blocking of CXCR2, the cognate receptor of CXCL5, diminishes aggressiveness and induces senescence through infiltration of tumor-associated macrophages (47). A prominent role of CXCL5 has been suggested previously in PC (29) and in breast cancer bone metastasis (48, 49). CXCL5 is detected in both immune and nonimmune cells including osteoblasts, endothelial cells, and fibroblasts (28). The underlying mechanism of CXCL5 induction is cell type dependent and regulated by environmental cues. Our study sheds light on this phenomenon and demonstrates the relevance of BM-MSCs within the bone marrow environment and confirms the contributions of both tumor and nontumor cells (including immune/nonimmune) as sources of CXCL5.

In addition to their roles in tissue regeneration and wound healing, BM-MSCs have tumor-tropic characteristics that promote tumor growth and cancer progression (50). Coculture of gastric or breast cancer cell lines with MSCs enhances directional migration and metastatic potential in vivo through paracrine signals and close physical contact (51, 52). Consistent with this supportive role, our study explains how BM-MSCs are educated to produce a favorable environment for metastatic outgrowth. During invasion into bone, tumor cells cross-talk with bone resident cells creating a favorable niche through secretion of growth factors, thereby providing an optimum setting to establish bone metastasis (53). Ex vivo implanted tumor cells (breast cancer) infiltrate into bone marrow and home to stromal cells confirming the relationship between tumor and bone stromal cells (54, 55). Experimental data suggests that the tumor cell-derived growth factor PDGF-AA acts directly on BM-MSCs to promote chemokine CXCL5 production. However, whether physical appearance of tumor cells in the niche are required need to be determined.

PDGFs are potent mitogens for mesenchymal stromal cells and associate in various physiological [tissue remodeling, wound healing (56)] and pathological (metastasis and tumor survival) functions (57). PDGFs could be produced by both tumor or nontumor cells (e.g., endothelial, macrophage), and both tumor and stromal cells such as blood vessels, fibroblasts, and myofibroblasts express PDGFR (α or β) receptors (57). Accordingly, expression of PDGFR in stroma may be a relevant regulator of fibroblast growth and a contributor to tumor progression and treatment response (58). We demonstrate that tumor cell–derived PDGF-AA induces CXCL5 through

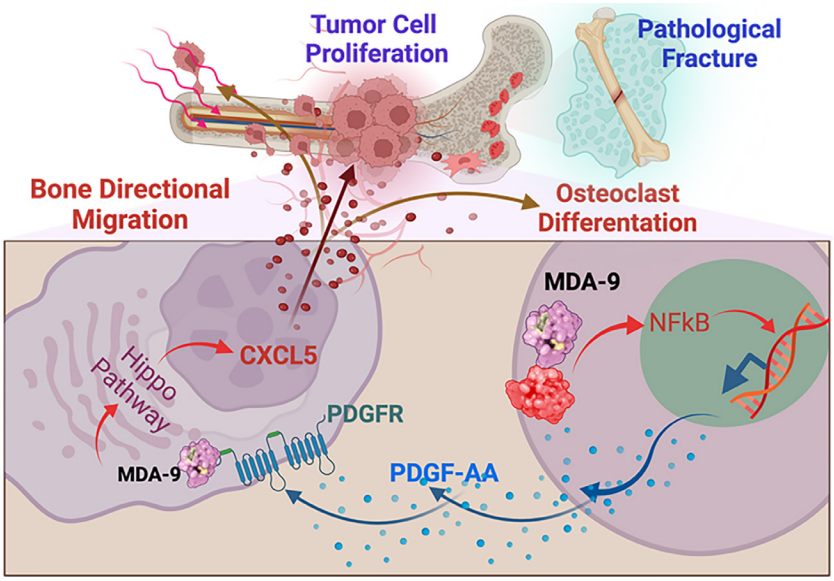

Fig. 9. Schematic of the proposed role of MDA-9 in BM-MSCs in creating a favorable environment for metastatic outgrowth through secretion of CXCL5 in response to tumor cell–derived growth factor, PDGF-AA.

activation of the intracellular Hippo pathway. PDGF-mediated activation of the Hippo pathway is evident in pancreatic stellate cells during experimental pancreatitis (by repeated cerulenin administration in wild-type mice) and initiation of neoplastic transformation of the pancreas parenchymain transgenic animals (59). Pharmacological inhibition or genetic silencing of PDGFR in cholangiocarcinoma also supports a role of PDGF in the Hippo signaling pathway (60). Activation of YAP transcription factor is a signature feature of cancer-associated fibroblasts (CAFs), a highly abundant and heterogeneous population of cells of mesenchymal lineage (61). In the tumor microenvironment, tumor cell–derived PDGF-AA, one of five members of PDGF family protein attracts MSCs, which are distinct from CAFs (62), and activate BMP-Smad1/ 5/8 pathway that leads to osteogenic differentiation (63). Targeting PDGF was not very successful in the clinic (64–67). Multikinase inhibitors that target PDGFR, such as Imatinib or Sunitinib, combined with salvage radiotherapy have not improved survival (64–66), and Tandutinib (67) promoted worse outcomes. A more accurate understanding of the underlying pathways and development of therapeutic approaches are therefore essential and inhibiting the ligands (e.g., PDGF) might be worth evaluating clinically.

The ability of MDA-9 to activate the Hippo pathway is an intriguing phenomenon. PDGFR-β harbors a PDZ-interacting motif and is documented to interact with PDZ domain proteins such as NHERF (68), RGS12 (69). These interactions control the cytoskeleton and the p44/42 MAPK pathways, respectively. In these contexts, it is possible that MDA-9 could interact with PDGFR and provide stability to induce PDGF signaling as we observed in other circumstances [e.g., activation of VEGFR2 (70) or IGF-1R (18) in endothelial and PC cells, respectively]. Our data using shRNA and KO BM-MSCs support MDA-9 as essential to translocation of YAP, which might occur by MDA-9 affecting YAP stability.

MDA-9 plays seminal roles in both the tumor and microenvironment (17, 19, 20), mediating cancer chemosensitivity (71), stem cell renewal (72), and tumor angiogenesis, invasion, and metastasis in many cancers (16, 17), predicting that targeting strategies might potentially lead to effective anticancer therapies. In recent years, interest has been devoted to targeting MDA-9 using pharmacological tools, including chemical- or peptide-based approaches (16). Using fragment-based drug discovery informed my NMR, we developed a pharmacological inhibitor that binds to the PDZ1 domain of MDA-9, PDZ1i (73, 74). It is conceivable that PDZ1i could block the physical interactions of MDA-9 with partners that are pivotal for PDGF-AA-mediated CXCL5 expression in bone, thereby preventing metastatic progression as observed previously (19). Comprehensive research including in vivo PK and safety assessment, formulation, and target distribution is needed in order to progress small-molecule MDA-9 PDZ inhibitors from bench to bedside.

Materials and Methods

Cell Lines. The human bone marrow–derived mesenchymal stromal cell line HS5 was obtained from the ATCC and was maintained in Dulbecco's Modified Eagle Medium (DMEM) supplemented with 10% fetal bovine serum and antibiotics. PC-3ML-*Luc* cells were obtained from M.G. Pomper (Johns Hopkins Medical Institutions, Baltimore, MD) and maintained as previously described (39). Murine prostate cancer cell line RM1 was provided by T.C. Thompson (Baylor College of Medicine, Houston, TX), and RM1-BM cells (derived from C57BL/6 J mouse bone metastases) were maintained in DMEM supplemented with 10% fetal bovine serum as previously described (34). Stable MDA-9/Syntenin knock-out clones were generated using sgRNA/Cas9 all-in-one expression clone targeting SDCBP (*mda-9/syntenin*) (Cat No: HCP216662-CG01-1) from GeneCopoeia. At 48 h posttransfection, cells were incubated with 5 mg/mL Neomycin to select resistant clones, and lack of MDA-9/Syntenin expression was confirmed by western blotting analysis. All cell lines were regularly monitored (once every 3 mo) for mycoplasma contamination using a mycoplasma detection kit (Sigma). Bone marrow stromal cells (BM-MSCs) were isolated from WT and *mda-9*$^{-/-}$ mice according to a previously described protocol (75).

Reagents and Antibodies. MDA-9/Syntenin (SDCBP) antibody was obtained from Abnova Inc. Antibodies for MST1, phosphor MST1, YAP, phosphor YAP, PDGFR-α, phospho-PDGFR-α and β-actin were purchased from Cell Signaling Technology. Fluorophore conjugated antibodies for various cell-surface markers, CD90, CD105, CD11b/mac, NK1.1 were obtained from eBioscience. CXCL5-AF700 were purchased from Novus Biologicals. Neutralizing antibodies for CXCL5 and PDGF-AA were obtained from R&D Systems. Human and mouse specific recombinant protein CXCL5, PDGF-AA, GM-CSF were procured from R&D Systems. MST overexpression and catalytically inactive pJ3M-Mst1 K59R were purchased from Addgene (43). YAP1 shRNA plasmids were obtained from GeneCopoeia, Inc. NF-κB inhibitor IKK2i was purchased from Sigma-Aldrich.

Promoter Assays. Promoter reporter clone of human CXCL5 (HPRM44649) in a custom PGL4 clone was obtained from GeneCopoeia, Inc. Transient transfection and luciferase assays in HS5 cells were performed using a previously described protocol (39).

ELISA. Human and mouse specific ELISA Kits for CXCL5 and PDGF-AA were purchased from R&D Systems. All ELISAs were performed using the manufacturer's protocol.

Invasion Assays. Boyden chamber assays were used to evaluate the invasive properties of cancer cells. Corning® BioCoat® Matrigel® Invasion Chambers with 8.0 μm PET Membrane were obtained from Corning Inc. Briefly, cells were plated on the Matrigel-coated upper chamber. After 18 h, invasive cells were fixed and stained in the lower chamber and were photographed and analyzed.

Real-Time PCR. Total RNA was extracted from cells using miRNeasy kits (Qiagen), and cDNA was prepared as described (18). TaqMan (Applied Biosystems) probes were used for specific gene expressions, and quantitative qPCR was performed using an ABI Quant Studio real-time PCR.

Antibody Array. Mouse Chemokine Antibody Array (ARY020) was purchased from R&D Systems. Human Growth Factor Array C1 (AAH-GF-1-4) was obtained from Ray Biotech Life. All antibody arrays were performed according to the manufacturer's protocol. Heat map was generated using Morpheus (https://software.broadinstitute.org/morpheus).

Flow Cytometric Analysis. The bone marrow was isolated from naive and tumor cells implanted (I.C or I.T) C57BL/6 *mda-9*^{WT} and *mda-9*$^{-/-}$. After RBC lysis (RBC Lysis buffer eBioscience), bone marrow cells were resuspended in FACS buffer (phosphate-buffered saline (PBS) containing 0.1% bovine serum albumin (BSA)). Surface staining was done with indicated antibodies, and for intracellular staining, samples were fixed by IC-Fixation buffer (eBioscience), permeabilized by permeabilization buffer (eBioscience) according to the manufacturer's protocol, and stained with the indicated antibodies. Stained cells were isolated and analyzed by BD FACS DIVA software in LSR-II flow cytometer (BD Biosciences).

Immunofluorescence (IF) and Immunohistochemistry (IHC). Bone sections were fixed in PBS–Formalin and then decalcified (10% ethylenediaminetetraacetic acid (EDTA), pH 6.5) for a total of 2 wk and placed into 70% ethanol before sectioning. Paraffin-embedded tissues were used for IHC and IF studies as described previously (76).

Clinical Tumor Samples. The laboratory information system in the Department of Pathology at the VCU Medical Center was queried for archived samples of metastatic prostate carcinoma involving the femur or spine between 2003 and 2021. A total of 29 samples were eligible for inclusion. The formalin-fixed paraffin-embedded tissue blocks were retrieved, and one hematoxylin and eosin section taken from each block was stained and reviewed by a board-certified anatomic pathologist to verify the diagnosis and quantity of tumor. Following review, 25 samples contained adequate tumor for study. Unstained slides were sectioned at 5 μm for immunohistochemical (IHC) staining with CXCL5.

Clinical Serum Samples. Deidentified serum samples were obtained from patients following informed consent and use of Institutional Review Board approved protocols at Eastern Virginia Medical School (IRB # 00-09-EX-0417) with patient eligibility as previously described: male donors aged 50 to 90 y; sample collection after January 1, 2002, using standard serum collection protocols, with storage at −80 °C within 4 h of collection; and samples subjected to at most one previous thaw. Eligible samples were selected randomly to achieve greatest balance by age and race. Deidentified patient information was used to classify samples into three diagnostic groups: 1) control group with diagnosis confirmed as benign prostatic hyperplasia (BPH) without cancer; 2) PC cases with pathological Gleason Grade score ≥7; and 3) PC with confirmed bone metastasis (Pathological Gleason Grade Score ≥ 7). The number of samples was 20 for each group (BPH and advanced PC with or without bone metastasis).

Bone Morphometry analysis. Femurs were fixed with 10% neutral buffered formalin prior to performing μCT as described previously (36). Bone volume (mm^3) was calculated by isolating all bone within three pixels of the outer three-dimensional surface of the implant. Bone volume was divided by the outer three-dimensional surface of the implant for calculating the bone volume over total volume (BV/TV).

Animal Studies. All animal studies and care were performed under the guidelines of the Virginia Commonwealth University Institutional Animal Care and Use Committee (IACUC), in accordance with the principles and procedures outlined in the National Research Council "Guide for the Care and Use of Laboratory Animals." Where needed, the animals were euthanized following the procedures approved by the VCU Institutional Animal Care and Use Committee under protocol AM10183 and consistent with the recommendations of the "American Veterinary Medical Association Guidelines for the Euthanasia of Animals: 2020 Editions".

***mda-9/syntenin* Knockout Mice.** *Mda-9/syntenin* "knockout first" mice (*Sdcbp*$^{tm1a(KOMP)Wtsi}$) were originally obtained from the Knockout Mouse Project (KOMP) Repository (20) and subsequently bred to mice expressing FLPe in the germline and then to mice expressing Cre in the germline to generate the global knockout allele, as described previously (20).

Intracardiac (I.C.) Cancer Cell Implantation. For experimental bone metastasis assays, 30,000 RM1-BM-*Luc* cells were injected by the intracardiac route to develop bone metastases in 6- to 8-wk-old male WT and *mda-9*$^{-/-}$ mice as described previously (n = 10) (20). The incidence of metastasis was monitored using bioluminescence imaging, as described previously (20). For "survival studies," animals were closely monitored and euthanized when they reached any of the humane endpoint criteria defined in our approved IACUC protocol.

Intrafemoral (I.F.) Cancer Cell Implantation. Six- to eight-week-old male C57BL/6 WT and *mda-9*$^{-/-}$ mice were used for this study. In brief, mice were anesthetized by isoflurane inhalation. The hind limbs were cleaned with betadine followed by 70% ethanol. A superficial incision was made in the skin lateral to the patella. Using a #4 water-cooled dental burr, a cavity was made in the diaphysis of the distal femur to allow access to the marrow cavity. Marrow was evacuated from the distal canal by repeated irrigation with saline solution. Using a micropipette, 10,000 RM1-BM-*Luc* cells suspended in 10 μL of PBS solution were injected into the medullary defect. The defect was sealed with bone wax to prevent evacuation of cancer cells. The surrounding muscle was reapproximated and sutured with a resorbable suture, and the skin was subsequently closed with a nylon suture. The animals were placed in a recovery chamber located on a heating pad and, following full recovery, were returned to their cages. The incidence of tumor cell growth in the bone was monitored by bioluminescence imaging.

Intracardiac Cancer Cell Implantation in Nude Mice. A total of 50,000 PC3-ML-*Luc* and PC3-ML$^{mda\text{-}9\ KO}$-*Luc* cells were implanted I.C. in 6- to 8-wk-old male athymic nude mice. The incidence of bone metastasis was monitored by bioluminescence imaging.

Autologous Bone Marrow Transfusion Study. Total bone marrow cells were isolated from femurs and tibias of 8-wk-old male C57BL/6 (donor) mice and passed through a 70-μM mesh cell strainer before infusing into the recipient mice, both WT and *mda-9*$^{-/-}$ (irradiated with a total of 10 Gy from a cesium irradiator). Eight weeks after transplantation, tumor cells were inoculated by intracardiac injection to develop bone metastases, as described above.

CXCL5 Neutralization Study. RM-1BM-*Luc* cells were implanted I.C. or I.T. into 6- to 8-wk-old C57BL/6 male mice. Mice were treated with three doses (30 μg/mouse) of either control IgG antibody or mouse CXCL5 neutralizing antibody (R&D system) intraperitoneally. The incidence of tumor cell growth in the bone was monitored by bioluminescence imaging.

Statistical Analysis. Data are presented as the mean ± SD and analyzed for statistical significance using the Student *t* test or ANOVA test in comparison with corresponding controls followed by the Newman–Keuls test as a post hoc test. $P < 0.05$ was considered statistically significant. Survival curves were analyzed using Cox proportional hazards survival regression using GraphPad Prism.

Data, Materials, and Software Availability. All study data are included in the article and/or *SI Appendix*.

ACKNOWLEDGMENTS. The present study was supported in part by NIH/National Cancer Institute (NCI) Grants R01 CA244993 (to D.S. and P.B.F.), RO1 Funding, CA259599 (to P.B.F. and X-Y.W.) and CA229812 (to X.-Y.W.); NCI Cancer Center Support Grant to the Virginia Commonwealth University (VCU) Massey Comprehensive Cancer Center (MCC) P30 CA016059 (to Robert Winn); and the National Foundation for Cancer Research (P.B.F.). P.B.F. holds the Thelma Newmeyer Corman Chair in Cancer Research at the MCC. D.S. is the Harrison Foundation Distinguished Professor in Cancer Research at the MCC. X.-Y.W. holds

the Harry and Judy Wason Chair in Cancer Research at the MCC. This research was also facilitated by the VCU/MCC Flow Cytometry Shared Resource and VCU/MCC Transgenic/Knockout Mouse Shared Resource, supported, in part, with funding from NIH/NCI Cancer Center Support Grant P30 CA016059.

Author affiliations: [a]Department of Human and Molecular Genetics, Virginia Commonwealth University, School of Medicine, Richmond, VA 23298; [b]VCU Institute of Molecular Medicine, Virginia Commonwealth University, School of Medicine, Richmond, VA 23298; [c]VCU Massey Comprehensive Cancer Center, Virginia Commonwealth University, School of Medicine, Richmond, VA 23298; [d]Department of Microbiology and Molecular Cell Biology, Eastern Virginia Medical School, Norfolk, VA 23507; [e]Department of Biostatistics, Virginia Commonwealth University, School of Medicine, Richmond, VA 23238; [f]Department of Internal Medicine, Virginia Commonwealth University, School of Medicine, Richmond, VA 23238; [g]Department of Pathology, Virginia Commonwealth University, School of Medicine, Richmond, VA 23238; [h]Department of Biomedical Engineering, College of Engineering, Virginia Commonwealth University, Richmond, VA 23238; [i]Department of Surgery, Virginia Commonwealth University, School of Medicine, Richmond, VA 23238; and [j]Ludwig Institute for Cancer Research, University of California San Diego, La Jolla, CA 92093

Author contributions: S.M., A. K. Pradhan, A. K. Paul, S.K.D., and P.B.F. designed research; S.M., A. K. Pradhan, A.K., P.B., P.M., C.G., M.M.L., and D.J.C. performed research; A. K. Pradhan, A.K., C.G., J.J.W., M.A.S., X.-Y.W., O.J.S., J.O.N., A. K. Paul, E.M., D.J.C., and R.G. contributed new reagents/analytic tools; S.M., A. K. Pradhan, X.-Y.W., N.M., B.H., D.S., L.E., S.K.D., and P.B.F. analyzed data; and S.M., W.K.C., S.K.D., and P.B.F. wrote the paper.

1. J. Rigaud *et al.*, Prognostic value of bone scan in patients with metastatic prostate cancer treated initially with androgen deprivation therapy. *J. Urol.* **168**, 1423–1426 (2002).
2. L. Ye, H. G. Kynaston, W. G. Jiang, Bone metastasis in prostate cancer: Molecular and cellular mechanisms (Review). *Int. J. Mol. Med.* **20**, 103–111 (2007).
3. C. Coghlin, G. I. Murray, Current and emerging concepts in tumour metastasis. *J. Pathol.* **222**, 1–15 (2010).
4. S. S. Ganguly, X. Li, C. K. Miranti, The host microenvironment influences prostate cancer invasion, systemic spread, bone colonization, and osteoblastic metastasis. *Front Oncol.* **4**, 364 (2014).
5. S. G. Pneumaticos *et al.*, Osteoprotegerin expression during the micro- and macrometastatic phases of the osteoblastic metastasis in prostate cancer: Therapeutic implications. *Expert Opin. Ther Targets* **17**, 1395–1403 (2013).
6. M. Croset, C. Kan, P. Clezardin, Tumour-derived miRNAs and bone metastasis. *Bonekey Rep.* **4**, 688 (2015).
7. S. Nandana, L. W. Chung, Prostate cancer progression and metastasis: Potential regulatory pathways for therapeutic targeting. *Am. J. Clin. Exp. Urol.* **2**, 92–101 (2014).
8. K. Jung, M. Lein, Bone turnover markers in serum and urine as diagnostic, prognostic and monitoring biomarkers of bone metastasis. *Biochim. Et Biophys. Acta-Rev. Cancer* **1846**, 425–438 (2014).
9. J. J. Grootjans *et al.*, Syntenin, a PDZ protein that binds syndecan cytoplasmic domains. *Proc. Natl. Acad. Sci. U.S.A.* **94**, 13683–13688 (1997).
10. J. J. Lin, H. Jiang, P. B. Fisher, Melanoma differentiation associated gene-9, mda-9, is a human gamma interferon responsive gene. *Gene* **207**, 105–110 (1998).
11. J. J. Lin, H. P. Jiang, P. B. Fisher, Characterization of a novel melanoma differentiation-associated gene, mda-9, that is down-regulated during terminal cell differentiation. *Mol. Cellular Differentiation* **4**, 317–333 (1996).
12. S. K. Das *et al.*, Raf kinase inhibitor RKIP inhibits MDA-9/Syntenin-mediated metastasis in melanoma. *Cancer Res.* **72**, 6217–6226 (2012).
13. S. K. Das *et al.*, MDA-9/Syntenin and IGFBP-2 promote angiogenesis in human melanoma. *Cancer Res.* **73**, 844–854 (2013).
14. H. Boukerche *et al.*, mda-9/Syntenin: A positive regulator of melanoma metastasis. *Cancer Res.* **65**, 10901–10911 (2005).
15. H. Boukerche, Z. Z. Su, C. Prevot, D. Sarkar, P. B. Fisher, mda-9/Syntenin promotes metastasis in human melanoma cells by activating c-Src. *Proc. Natl. Acad. Sci. U.S.A.* **105**, 15914–15919 (2008).
16. S. K. Das, D. Sarkar, L. Emdad, P. B. Fisher, MDA-9/Syntenin: An emerging global molecular target regulating cancer invasion and metastasis. *Adv. Cancer Res.* **144**, 137–191 (2019).
17. A. K. Pradhan *et al.*, MDA-9/Syntenin/ SDCBP: New insights into a unique multifunctional scaffold protein. *Cancer Metastasis Rev.* **39**, 769–781 (2020).
18. S. K. Das *et al.*, The MDA-9/Syntenin/IGF1R/STAT3 axis directs prostate cancer invasion. *Cancer Res.* **78**, 2852–2863 (2018).
19. S. K. Das *et al.*, Suppression of prostate cancer pathogenesis using an MDA-9/Syntenin (SDCBP) PDZ1 small molecule inhibitor. *Mol. Cancer Ther.* **18**, 1997–2007 (2019).
20. S. K. Das *et al.*, Knockout of MDA-9/Syntenin (SDCBP) expression in the microenvironment dampens tumor-supporting inflammation and inhibits melanoma metastasis. *Oncotarget* **7**, 13 (2016).
21. A. Alphonso, S. K. Alahari, Stromal cells and integrins: Conforming to the needs of the tumor microenvironment. *Neoplasia* **11**, 1264–1271 (2009).
22. P. G. Corn, The tumor microenvironment in prostate cancer: Elucidating molecular pathways for therapy development. *Cancer Manag Res.* **4**, 183–193 (2012).
23. A. F. Olumi *et al.*, Carcinoma-associated fibroblasts direct tumor progression of initiated human prostatic epithelium. *Cancer Res.* **59**, 5002–5011 (1999).
24. R. Singh, J. W. Lillard Jr., S. Singh, Chemokines: Key players in cancer progression and metastasis. *Front Biosci. (Schol Ed)* **3**, 1569–1582 (2011).
25. S. J. Coniglio, Role of tumor-derived chemokines in osteolytic bone metastasis. *Front Endocrinol.* **9**, 313 (2018).
26. G. Nishikawa *et al.*, Bone marrow-derived mesenchymal stem cells promote colorectal cancer progression via CCR5. *Cell Death & Dis.* **10**, 264 (2019).
27. G. Ren, M. Esposito, Y. Kang, Bone metastasis and the metastatic niche. *J. Mol. Med.* **93**, 1203–1212 (2015).
28. H. W. Wen Zhang *et al.*, CXCL5/CXCR2 axis in tumor microenvironment as potential diagnostic biomarker and therapeutic target. *Cancer Commun. (Lond)* **40**, 69–80 (2020).
29. H. Roca *et al.*, Apoptosis-induced CXCL5 accelerates inflammation and growth of prostate tumor metastases in bone. *J. Clin. Invest.* **128**, 248–266 (2018).
30. L. A. Begley *et al.*, CXCL5 promotes prostate cancer progression. *Neoplasia* **10**, 244–254 (2008).
31. K. Yildirim *et al.*, Clinical value of CXCL5 for determining of colorectal cancer. *Asian Pac. J. Cancer Prev.* **19**, 2481–2484 (2018).
32. K. Wu *et al.*, The clinical significance of CXCL5 in non-small cell lung cancer. *OncoTargets Therapy* **10**, 5561–5573 (2017).
33. S. L. Zhou *et al.*, Overexpression of CXCL5 mediates neutrophil infiltration and indicates poor prognosis for hepatocellular carcinoma. *Hepatology* **56**, 2242–2254 (2012).
34. C. Guo *et al.*, In situ vaccination with CD204 gene-silenced dendritic cell, not unmodified dendritic cell, enhances radiation therapy of prostate cancer. *Mol. Cancer Ther* **11**, 2331–2341 (2012).
35. C. A. Power *et al.*, A novel model of bone-metastatic prostate cancer in immunocompetent mice. *Prostate* **69**, 1613–1623 (2009).
36. D. J. Cohen, V. Patel, A. Verma, B. D. Boyan, Z. Schwartz, Effect of 17beta-estradiol on estrogen receptor negative breast cancer cells in an osteolytic mouse model. *Steroids* **142**, 28–33 (2019).
37. J. Li *et al.*, Human fucosyltransferase 6 enables prostate cancer metastasis to bone. *Br J. Cancer* **109**, 3014–3022 (2013).
38. B. W. Simons *et al.*, A mouse model of prostate cancer bone metastasis in a syngeneic immunocompetent host. *Oncotarget* **10**, 6845–6854 (2019).
39. A. Bhatnagar *et al.*, AEG-1 promoter-mediated imaging of prostate cancer. *Cancer Res.* **74**, 5772–5781 (2014).
40. A. K. Pradhan *et al.*, Recombinant MDA-7/IL24 suppresses prostate cancer bone metastasis through downregulation of the Akt/Mcl-1 pathway. *Mol. Cancer Therapeutics* **17**, 1951–1960 (2018).
41. G. Wang *et al.*, Targeting YAP-dependent MDSC infiltration impairs tumor progression. *Cancer Discov* **6**, 80–95 (2016).
42. A. Adamo *et al.*, HS-5 and HS-27A stromal cell lines to study bone marrow mesenchymal stromal cell-mediated support to cancer development. *Front Cell Dev. Biol.* **8**, 584232 (2020).
43. C. L. Creasy, D. M. Ambrose, J. Chernoff, The Ste20-like protein kinase, Mst1, dimerizes and contains an inhibitory domain. *J. Biol. Chem.* **271**, 21049–21053 (1996).
44. G. Battafarano, M. Rossi, F. Marampon, A. Del Fattore, Cellular and molecular mediators of bone metastatic lesions. *Int. J. Mol. Sci.* **19**, 80–95 (2018).
45. A. M. Muscarella, S. Aguirre, X. Hao, S. M. Waldvogel, X. H. Zhang, Exploiting bone niches: Progression of disseminated tumor cells to metastasis. *J. Clin. Invest.* **131**, e143764 (2021).
46. E. Madan *et al.*, Cell competition in carcinogenesis. *Cancer Res.* **82**, 4487–4496 (2022), 10.1158/0008-5472.CAN-22-2217.
47. X. Li *et al.*, A destructive cascade mediated by CCL2 facilitates prostate cancer growth in bone. *Cancer Res.* **69**, 1685–1692 (2009).
48. R. Romero-Moreno *et al.*, The CXCL5/CXCR2 axis is sufficient to promote breast cancer colonization during bone metastasis. *Nat. Commun.* **10**, 4404 (2019).
49. Y. H. Yang *et al.*, Semaphorin 4D promotes skeletal metastasis in breast cancer. *PLoS One* **11**, e0150151 (2016).
50. M. Quante *et al.*, Bone marrow-derived myofibroblasts contribute to the mesenchymal stem cell niche and promote tumor growth. *Cancer Cell* **19**, 257–272 (2011).
51. Z. Xue *et al.*, Mesenchymal stem cells promote epithelial to mesenchymal transition and metastasis in gastric cancer though paracrine cues and close physical contact. *J. Cell Biochem.* **116**, 618–627 (2015).
52. K. M. McAndrews, D. J. McGrail, N. Ravikumar, M. R. Dawson, Mesenchymal Stem Cells Induce Directional Migration of Invasive Breast Cancer Cells through TGF-beta. *Sci. Rep.* **5**, 16941 (2015).
53. N. Graham, B. Z. Qian, Mesenchymal stromal cells: Emerging roles in bone metastasis. *Int. J. Mol. Sci.* **19**, 1121 (2018).
54. M. T. Haider, I. Holen, T. N. Dear, K. Hunter, H. K. Brown, Modifying the osteoblastic niche with zoledronic acid in vivo-potential implications for breast cancer bone metastasis. *Bone* **66**, 240–250 (2014).
55. H. Wang *et al.*, The osteogenic niche promotes early-stage bone colonization of disseminated breast cancer cells. *Cancer Cell* **27**, 193–210 (2015).
56. T. O. Tokunaga *et al.*, PDGF receptor β is a potent regulator of mesenchymal stromal cell function. *J. Bone Miner Res.* **23**, 9 (2008).
57. A. A. Farooqi, Z. H. Siddik, Platelet-derived growth factor (PDGF) signalling in cancer: Rapidly emerging signalling landscape. *Cell Biochem. Funct.* **33**, 257–265 (2015).
58. R. Catena *et al.*, PDGFR signaling blockade in marrow stroma impairs lung cancer bone metastasis. *Cancer Res.* **71**, 164–174 (2011).
59. C. Hu *et al.*, Yes-associated protein 1 plays major roles in pancreatic stellate cell activation and fibroinflammatory responses. *Front Physiol.* **10**, 1467 (2019).
60. R. L. Smoot *et al.*, Platelet-derived growth factor regulates YAP transcriptional activity via Src family kinase dependent tyrosine phosphorylation. *J. Cell Biochem.* **119**, 824–836 (2018).
61. V. S. LeBleu, R. Kalluri, A peek into cancer-associated fibroblasts: Origins, functions and translational impact. *Dis. Model Mech.* **11**, dmm029447 (2018).
62. T. L. Watts *et al.*, PDGF-AA mediates mesenchymal stromal cell chemotaxis to the head and neck squamous cell carcinoma tumor microenvironment. *J. Transl. Med.* **14**, 337 (2016).
63. A. Li *et al.*, PDGF-AA promotes osteogenic differentiation and migration of mesenchymal stem cell by down-regulating PDGFRalpha and derepressing BMP-Smad1/5/8 signaling. *PLoS One* **9**, e113785 (2014).
64. P. Mathew *et al.*, Platelet-derived growth factor receptor inhibition and chemotherapy for castration-resistant prostate cancer with bone metastases. *Clin. Cancer Res.* **13**, 5816–5824 (2007).
65. A. Rosenberg, P. Mathew, Imatinib and prostate cancer: Lessons learned from targeting the platelet-derived growth factor receptor. *Expert Opin. Investig. Drugs* **22**, 787–794 (2013).
66. A. J. Armstrong *et al.*, A phase 2 multimodality trial of docetaxel/prednisone with sunitinib followed by salvage radiation therapy in men with PSA recurrent prostate cancer after radical prostatectomy. *Prostate Cancer Prostatic Dis.* **19**, 100–106 (2016).
67. P. Mathew *et al.*, Accelerated disease progression in prostate cancer and bone metastases with platelet-derived growth factor receptor inhibition: Observations with tandutinib. *Cancer Chemother. Pharmacol.* **68**, 889–896 (2011).

68. J. B. Demoulin *et al.*, Ligand-induced recruitment of Na+/H+-exchanger regulatory factor to the PDGF (platelet-derived growth factor) receptor regulates actin cytoskeleton reorganization by PDGF. *Biochem. J.* **376**, 505–510 (2003).
69. B. S. Sambi *et al.*, The effect of RGS12 on PDGFbeta receptor signalling to p42/p44 mitogen activated protein kinase in mammalian cells. *Cell Signal* **18**, 971–981 (2006).
70. N. Tae *et al.*, Syntenin promotes VEGF-induced VEGFR2 endocytosis and angiogenesis by increasing ephrin-B2 function in endothelial cells. *Oncotarget* **8**, 38886–38901 (2017).
71. S. Talukdar *et al.*, MDA-9/Syntenin (SDCBP) is a critical regulator of chemoresistance, survival and stemness in prostate cancer stem cells. *Cancers* **12**, E53 (2020).
72. S. Talukdar *et al.*, Novel function of MDA-9/Syntenin (SDCBP) as a regulator of survival and stemness in glioma cancer stem cells. *Oncotarget* **7**, 54102–54119 (2016).
73. T. Kegelman *et al.*, Inhibition of radiation-induced glioblastoma invasion by genetic and pharmacological targeting of MDA-9/Syntenin. *Proc. Natl. Acad. Sci. U.S.A.* **114**, 370–375 (2017).
74. S. K. Das, D. Sarkar, W. K. Cavenee, L. Emdad, P. B. Fisher, Rethinking glioblastoma therapy: MDA-9/Syntenin targeted small molecule. *ACS Chem. Neurosci.* **10**, 1121–1123 (2099).).
75. B. Nowlan, K. Futrega, E. D. Williams, M. R. Doran, Human bone marrow-derived stromal cell behavior when injected directly into the bone marrow of NOD-scid-gamma mice pre-conditioned with sub-lethal irradiation. *Stem Cell Res. Therapy* **12**, 231 (2021).
76. P. Bhoopathi *et al.*, Regulation of neuroblastoma migration, invasion, and in vivo metastasis by genetic and pharmacological manipulation of MDA-9/Syntenin. *Oncogene* **38**, 6781–6793 (2019).